Cloud Coverage in the Joint OSSE Nature Run

WILL MCCARTY

Global Modeling and Assimilation Office, NASA Goddard Space Flight Center, Greenbelt, Maryland

RONALD M. ERRICO

Goddard Earth Sciences Technology and Research Center, Morgan State University, Baltimore, and Global Modeling and Assimilation Office, NASA Goddard Space Flight Center, Greenbelt, Maryland

RONALD GELARO

Global Modeling and Assimilation Office, NASA Goddard Space Flight Center, Greenbelt, Maryland

(Manuscript received 1 June 2011, in final form 28 December 2011)

ABSTRACT

A successful observing system simulation experiment (OSSE) is fundamentally dependent on the simulation of the global observing system used in the experiment. In many applications, a free-running numerical model simulation, called a nature run, is used as the meteorological truth from which the observations are simulated. To accurately and realistically simulate observations from any nature run, the simulated observations must contain realistic cloud effects representative of the meteorological regimes being sampled. This study provides a validation of the clouds in the Joint OSSE nature run generated at ECMWF. Presented is the methodology used to validate the nature run cloud fraction fields with seasonally aggregated combined *CloudSat*/*Cloud–Aerosol Lidar and Infrared Pathfinder Satellite Observation* (*CALIPSO*) cloud geometric profile retrievals and the Wisconsin High Resolution Infrared Radiation Sounder (HIRS) cloud climatology. The results show that the Joint OSSE nature run has a correct vertical distribution of clouds but lacks globally in cloud amount compared to the validation data. The differences between the nature run and validation datasets shown in this study should be considered and accounted for in the generation of the global observing system for use in full OSSE studies.

1. Introduction

Even with advanced data assimilation techniques, the true atmospheric state is unknown and the analysis contains an error. An observing system simulation experiment (OSSE) is an attempt to generate simulated observations that mimic reality from an artificial truth for use in a mature data assimilation system. Called a *nature run*, the truth may be a free-running numerical model simulation with minimal knowledge of any realistic atmospheric state, but with a realistic climatology consisting of realistic weather patterns. While ideally this would contain features of all scales, the physical discretization of the atmosphere onto a grid of limited horizontal and vertical resolution limits atmospheric phenomena that can be characterized. This shortcoming must be compensated for when considering any feature that falls below those resolvable in the nature run itself.

The realistic simulation of observations from a nature run is essential to properly exercise a data assimilation system in the OSSE context. A properly simulated observation can be broken into two aspects. First, it must be simulated from the atmospheric state. This can be as simple as a four-dimensional interpolation to simulate a point measurement, such as a surface or single-level radiosonde observation, or a more complicated forward model combining multiple atmospheric variables into a single observation, such as putting an atmospheric state through a radiative transfer algorithm. Second, its inaccuracy must be appropriately characterized by an observation error. Fundamental to data assimilation, this error can be separated into multiple parts, including instrument noise and error of representativeness. Not unique to either the

Corresponding author address: Will McCarty, Goddard Space Flight Center, Mail Code 610.1, 8800 Greenbelt Rd., Greenbelt, MD 20771.
E-mail: will.mccarty@nasa.gov

DOI: 10.1175/MWR-D-11-00131.1

observation or its error are the effects from realistic, but not easily handled, atmospheric phenomena such as clouds. In data assimilation, cloud effects are typically considered a contamination to an observation, are treated as a source of error, and screened out of the assimilation process (Derber and Wu 1998; McNally and Watts 2003). As a potential source of unscreened error in data assimilation, simulated observations must realistically reflect the effects of clouds.

This study presents a validation of the cloud fields in the Joint OSSE nature run (NR) generated by the European Centre for Medium-Range Weather Forecasts (ECMWF; Andersson and Masutani 2010). This NR has been the basis of OSSE studies for a number of centers worldwide (Masutani et al. 2009), including the Global Modeling and Assimilation Office (GMAO) at the National Aeronautics and Space Administration (NASA) Goddard Space Flight Center. The NR has been generated using the ECMWF model (version cy31r1) at T511 resolution with 91 vertical levels above the surface. Initialized by the ECMWF operational analysis at 1200 UTC 1 May 2005 and integrated until 0000 UTC 1 June 2006, forecasted atmospheric states are available every 3 h on a reduced Gaussian grid. Beyond the initial analyzed state, the only information about the real atmospheric state over the integration period was in time-varying sea surface temperatures specified as lower boundary conditions.

Reale et al. (2007) presented verification on the tropical Atlantic and African monsoon regions within the NR, but further verification is necessary. This study illustrates the efforts at the GMAO to characterize the strengths and weaknesses in the placement and amount of clouds in the nature run relative to true observations of the clouds. For the purpose of this study, the December–February (DJF) months of the nature run are considered, as they correspond to efforts under way at the GMAO that will be the basis for future OSSE studies.

2. Verification data

a. CloudSat *and* CALIPSO

The level-2 cloud geometrical profile with lidar product (2B-GEOPROF-lidar; Mace and Zhang 2008, hereafter CS/CAL) is the primary verification data used in this study. This product contains two-dimensional cloud profiles, vertically and along-track, determined by combining *CloudSat* Cloud Profiling Radar (CPR; Stephens et al. 2008) measurements and *Cloud–Aerosol Lidar and Infrared Pathfinder Satellite Observation* (*CALIPSO*) Cloud–Aerosol Lidar with Orthogonal Polarization (CALIOP; Winker et al. 2007) measurements. The multi-instrument approach combines the profiling capability of the CPR and the sensitivity to thin clouds of CALIOP. The product has an along-track resolution of 1 km and a vertical resolution of 240 m. Up to five cloud layers within a column are reported, defined by cloud base and height. For consistency among the datasets presented in this paper, atmospheric profiles derived from corresponding ECMWF global state variables and provided as an auxiliary product by the *CloudSat* Data Processing Center (ECMWF-AUX; Partain 2010) are used to convert the retrieved cloud-layer-top geometric heights to pressure heights. All temporally matched 2B-GEOPROF-lidar and ECMWF-AUX pairs available from the *CloudSat* Data Processing Center for the DJF seasons between 1 December 2006 and 28 February 2009 are considered in this study.

b. HIRS cloud climatology

The HIRS cloud climatology (Wylie et al. 1994; Wylie and Menzel 1999) is also used for verification in this study. For this product, the CO_2 slicing method (Smith and Platt 1978; Menzel et al. 1983) for solving cloud-top pressure (CTP) has been applied to measurements from the High Resolution Infrared Radiation Sounder (HIRS) measurements and aggregated to develop climatological statistics. The HIRS instrument has flown operationally on the National Oceanic and Atmospheric Administration (NOAA) Polar Operational Environmental Satellites (POES) in both morning and afternoon orbits. For diurnal consistency between these data and the *CloudSat*/*CALIPSO* data, only statistics corresponding to the HIRS instruments on board NOAA afternoon orbit satellites—*NOAA-7*, *NOAA-9*, *NOAA-11*, *NOAA-14*, and *NOAA-16*—have been considered. These satellites have nominal local time of ascending node (LTAN) of 1400 local solar time, which closely corresponds to approximately 1330 LTAN of *CloudSat* and *CALIPSO*. No compensation for orbit drift (Price 1991) is made. This limited the period of consideration for these data to DJF seasons between December 1981 and 2001.

3. Processing

Because of the higher along-track resolution of the CS/CAL data compared with the horizontal grid spacing of the NR data, it is necessary to account for subgrid-scale variability in the latter. Similar to Chepfer et al. (2008), this study aims to compare the multiple datasets in a state that is intermediate between the nature run grid and observation scales. The NR cloud fractions are projected from the model domain to the observation scale before aggregating to larger sampling grids to establish robust distributions spatially for both. A maximum-random overlap scheme for clouds (Geleyn and Hollingsworth 1979; Wilkinson et al. 2008) is used to account for the difference

in NR grid spacing and CS/CAL product resolution, which differ by a factor of 39. Subgrid cloud formations that conserve the three-dimensional NR cloud fraction fields are generated at the spatial resolution of the CS/CAL product. Figure 1 illustrates on a horizontal plane how the subgrid is oriented within each model grid box. Subgrid cloud formations are generated to maximize overlap in vertically adjacent cloudy model levels. If the NR cloud fraction is zero (i.e., clear-sky conditions) between cloud fields in a vertical column, then the subgrid clouds are placed randomly. No vertical decorrelation length is considered. Disconnected cloud fields are oriented randomly if at least one clear-sky level exists between vertical formations. When randomly placed, circular cloud formations are generated about a randomly selected centroid to match the NR cloud fraction. The two-dimensional generation of clouds with a spatially continuous shape, like the circular growth implemented in this method, results in a nonconstant probability of cloud across the horizontal subgrid. The probability of cloud increases toward the center of the subgrid. Also, no horizontal correlations are considered beyond those at the subgrid scale. A generated subgrid formation has no information about the cloud fractions in horizontally adjacent grid boxes in the NR.

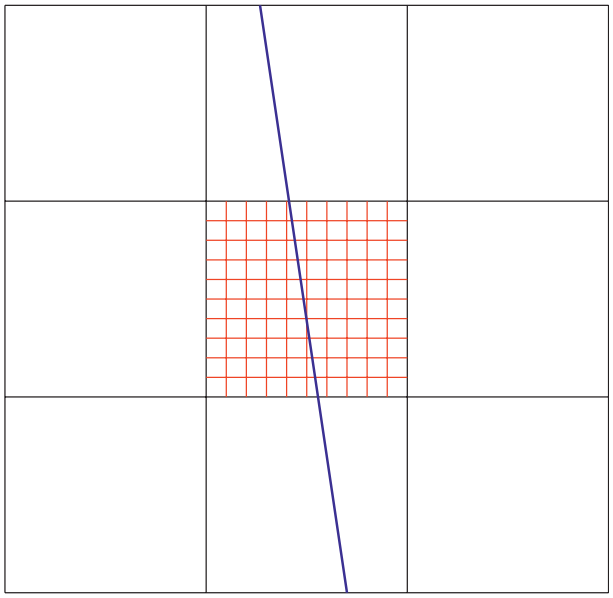

FIG. 1. Schematic illustrating the horizontal subgrid (red grid) relative to the full NR grid (black grid) at a single vertical level. Clouds are generated on the subgrid, conserving the cloud fraction defined at the NR resolution. The blue line represents the orientation of a CS/CAL overpass relative to the grid near the equator.

In addition to differences in the spatial resolution between the NR and verification data, there are also temporal discrepancies that need to be considered. The CS/CAL data are nearly continuous in time, with the temporal resolution of the product equating to 0.16-s sampling. The NR data, however, are only available every 3 h. Linear interpolation in time is inadequate, as the averaging of cloud fractions would bias the overall results toward clear sky as a result of the discontinuous nature of the fields. To compensate for this, a nearest-neighbor-in-time sampling of the NR is performed to collocate the data. While the sampling near the temporal midpoints of the NR data fields can result in discontinuities, it conserves the cloud fraction in a more appropriate manner than temporal interpolation.

Finally, all results presented in this study are based on *top-downward* calculations. Only the pressure–height of the highest cloud top in a given instantaneous scene is considered in both the CS/CAL and subgrid sampled NR data. This method is chosen to avoid incorporating an instrument model and retrieval algorithm on the NR data and to maintain consistency among the NR, CS/CAL, and HIRS data. This allows for the sampling of both high clouds and low clouds on the NR subgrid. The use of random overlap between vertically disconnected clouds allows for low clouds to be partially uncovered by the highest clouds on the subgrid. The CS/CAL data are susceptible to signal attenuation through clouds, which can limit their measurement of low clouds in multilayer profiles. The HIRS cloud climatology is based on the CO_2 slicing technique, which has no profiling capability. Therefore, considering the top of the highest clouds is consistent among all three data types. Also, no effort is made to consider cloud ice or liquid water amount. This biases the intercomparison, as the CS/CAL product has a minimum sensitivity to low amounts of cloud liquid or ice water content. Incorporating these variables would again require the incorporation of an instrument model and retrieval algorithm. As an active lidar, CALIOP has the highest sensitivity to optically thin clouds of all remotely sensed data in this study. The differences between the NR cloud fraction fields and observations shown in this study are greater than any bias imparted by low cloud water contents. It is noted that the aforementioned Chepfer et al. (2008) and Wilkinson et al. (2008) references differ from this study in that they incorporated instrument models in their intercomparison of model and lidar data.

4. Results

Nature run cloud fraction fields for DJF have been compared to climatologies generated from both the CS/CAL and HIRS products. Although validation of the NR over the entire integration period is desirable, including an analysis of interseasonal variations, this study

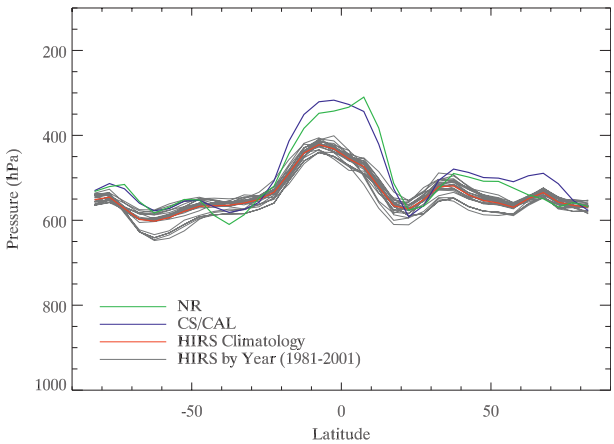

FIG. 2. Latitudinally averaged cloud-top pressure, binned every 5°, for the NR (green), CS/CAL (blue), and HIRS climatology (red). Each annual member of the HIRS climatology between 1981 and 2001 is shown in gray.

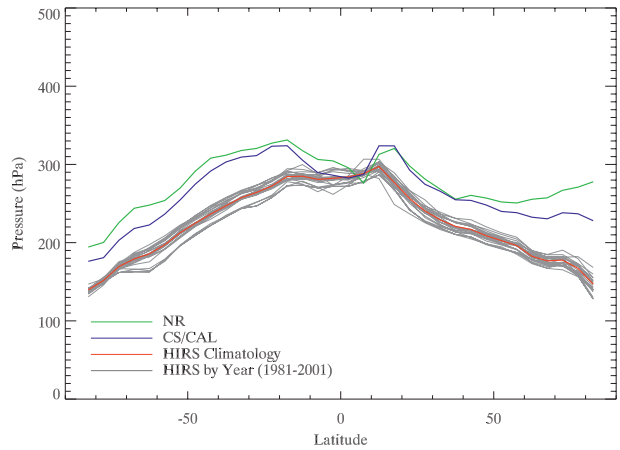

FIG. 3. Latitudinally averaged standard deviation of cloud-top pressure, calculated about the averages shown in Fig. 2.

is limited to the DJF time frame because it corresponds with a period under investigation in multiple studies at the GMAO. The methodologies presented in the previous section are used to sample the NR at CS/CAL resolution corresponding spatially and temporally to the orbit of the CS/CAL product[1] during the 1 December 2006–28 February 2007 time frame.

a. Cloud height in NR

The latitudinally averaged values of CTP for the NR, CS/CAL, and HIRS data are shown in Fig. 2. The values in the NR agree well with the CS/CAL observations at most latitudes. The global areal average values of CTP for the NR and CS/CAL are 482 and 490 hPa, respectively, as compared with 529 hPa for HIRS. The difference between the CS/CAL and HIRS values is expected because the HIRS product is based on infrared CTP retrievals. Weisz et al. (2007) showed that infrared-retrieved CTP was biased toward lower cloud heights (higher CTP) compared to CALIOP for both the Moderate Resolution Imaging Spectroradiometer (MODIS) and the Atmospheric Infrared Sounder (AIRS). In the subtropics and Southern Hemisphere midlatitudes, the CS/CAL and NR fall within the spread of the 23 individual years of HIRS data, with the only exception being data at 35°–40°S, where the NR average CTP is 28 hPa greater than CS/CAL and 45 hPa greater than HIRS. The NR and CS/CAL observations have lesser CTP values in the polar regions, tropics, and Northern Hemisphere midlatitudes compared with the HIRS climatology. The largest disagreement between the NR and HIRS is in the tropics, with a maximum difference of 163 hPa at 5°–10°N. The NR and CS/CAL data are more consistent with one another in the tropics, although the CTP values in the NR have a sharp peak near 10°N, while the CS/CAL values in the NR have a broad peak centered close to the equator. The NR and CS/CAL disagree most between 60° and 75°N, where the CTP in the NR is on average 53 hPa greater.

The *CloudSat*/*CALIPSO* product and the sampled NR data have much finer spatial resolutions than the HIRS climatology. As a result, the CS/CAL and NR datasets have a higher probability of measuring low clouds than does HIRS. The standard deviation of CTP as a function of latitude (Fig. 3) indicates that the NR and CS/CAL CTPs are globally more variant than the HIRS CTP. In the tropics, the variances are similar among all three datasets, indicating that the spread of the distribution of cloud-top pressures within the more finely sampled datasets is similar to that of the coarse HIRS measurements. The CTPs in the NR have somewhat higher variability than in the CS/CAL data, especially poleward of 50°.

b. Cloud fraction in the NR

The cloud amount in the nature run is as important to an OSSE as the cloud placement. Figure 4 shows cloud fraction as a function of latitude for the NR and CS/CAL data. For simplicity, cloud fractions are only considered for the NR data with the maximum-random overlap assumption and CS/CAL data with no submeasurement scale clouds. The latitudinal binning methodology is the same as in Fig. 2. Both datasets show similar latitudinal variations in cloud fraction, implying that the distribution of clouds in the NR is realistic, although the overall cloud amount is lacking. The NR measurements show fewer clouds at most latitudes, except poleward of 60°N

[1] The orbits of *CloudSat* and *CALIPSO* differ slightly. The geolocation provided in the product corresponds to *CloudSat*.

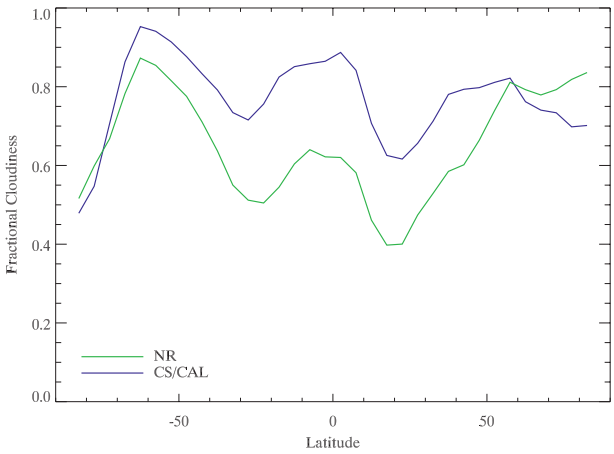

FIG. 4. Latitudinally averaged total cloud fraction, binned every 5°, for the NR (green) and CS/CAL (blue) data. Results plotted are for all clouds vertically.

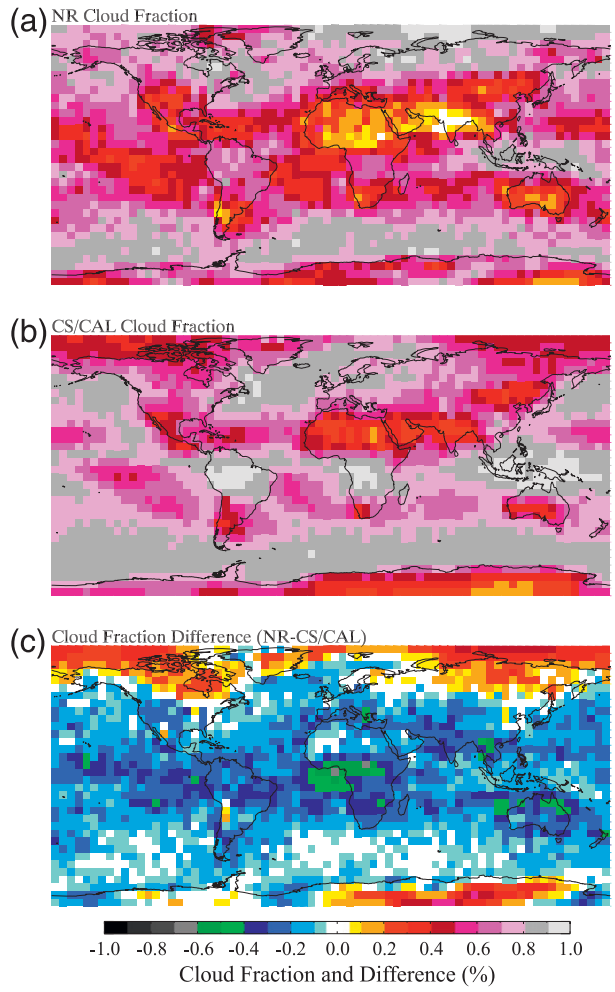

FIG. 5. Total cloud fraction, averaged over 5° by 5° boxes horizontally for the (a) NR and (b) CS/CAL data. (c) The difference, defined as NR − CS/CAL, is shown. Results shown are for all clouds vertically.

and 75°S. Between 30°S and 25°N, the NR underestimates cloud fraction by no less than 20% compared to the CS/CAL observations, with the largest difference being 28% at 20°–15°S. Both datasets indicate maxima in cloud fraction between 65° and 60°S and in the tropics, although the CS/CAL data have a local maximum between 0° and 5°N, while the NR peaks between 10° and 5°S. The differences between the local maxima differ strongly, as the CS/CAL data differ by 7% peak to peak, while the NR data differ by 23% peak to peak.

Globally, the average cloud fraction in the NR is 61.5% if maximum-random cloud overlap is assumed. The 3-yr CS/CAL globally averaged cloud fraction, assuming the highest clouds to be opaque, is 78.3%. The CS/CAL product does retrieve an estimation of cloud fraction below the measurement scale (Mace and Zhang 2008), and considering this quantity reduces the global cloud fraction to 74.5%. Subgrid-scale clouds in the NR data are determined only at the CS/CAL resolution and are considered binary, as in cloudy or clear. Therefore, it is appropriate to compare the values of 78.3% based on the CS/CAL data to the NR data with the maximum-random overlap assumption. The HIRS climatology was also considered, having a cloud fraction of 75.4%, but no effort was made to compensate for the differences in spatial resolution or submeasurement variability.

The differences seen in the latitudinal averages are further illustrated by considering the spatial distribution of cloud fraction. Figure 5 shows the cloud fraction for the CS/CAL and NR data, binned every 5° in both the zonal and meridional directions. The largest underestimation of clouds by the NR compared to CS/CAL is seen in the tropics at all longitudes, although the lack of clouds is also evident throughout the midlatitudes. In the polar regions, the differences vary in sign by longitude, indicating that the NR overrepresents and underrepresents cloud fraction regionally compared to CS/CAL. In general, the CS/CAL and NR data show better agreement in the Southern Hemisphere midlatitudes and polar regions than in the Northern Hemisphere, though large areal differences exist in both.

The vertical distribution of clouds can also significantly affect the simulation of observations in an OSSE. Figures 6, 7, and 8 show the cloud fraction fields for both the NR and CS/CAL data are separated into three layers, depicted as high-level (CTP < 440 hPa), midlevel (700 > CTP > 440 hPa), and low-level (CTP > 700 hPa) clouds, respectively, based on the International Satellite Cloud Climatology Project (ISSCP) classifications (Rossow and Schiffer 1991). The sum of the fractions for each layer classification in each 5° × 5° horizontal grid box

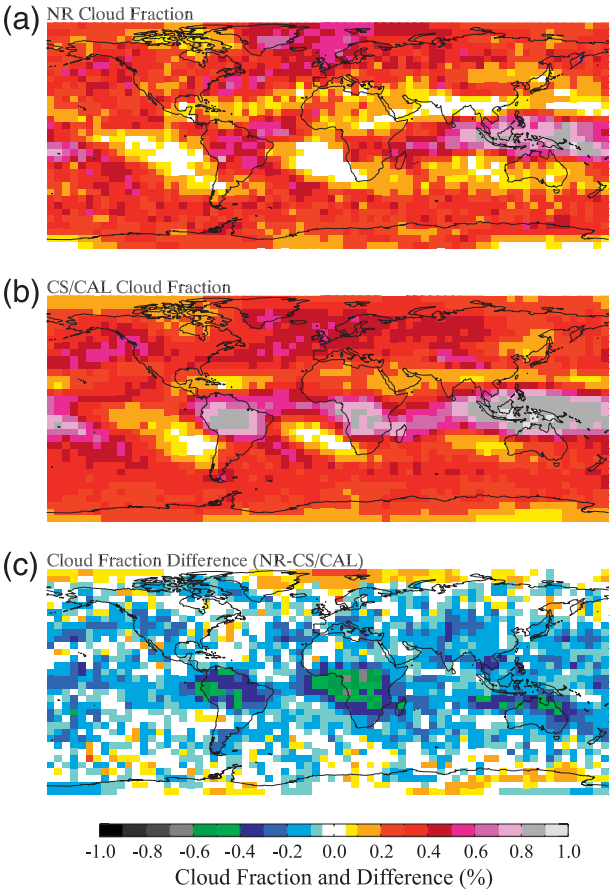

FIG. 6. As in Fig. 5, but for high-level clouds only, defined as those having a cloud-top pressure less than 440 hPa.

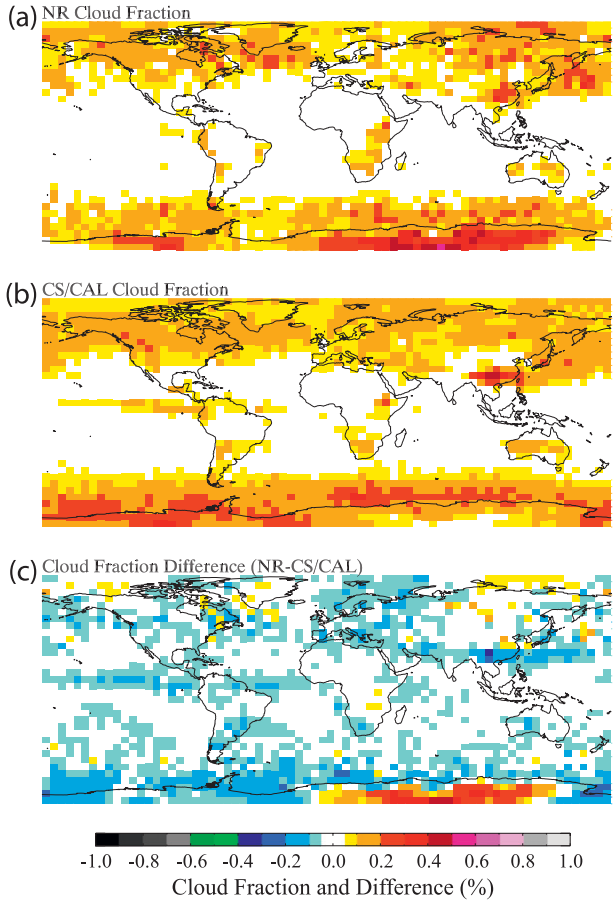

FIG. 7. As in Fig. 5, but for midlevel clouds, defined as those having a cloud-top pressure between 700 and 440 hPa.

corresponds to the values shown in Fig. 5. Considering the overall variability of the spatial plots, the largest cloud amounts in both the CS/CAL and NR data are seen in the upper levels. This is to be expected because of the top-downward approach used in this analysis. Midlevel clouds are confined primarily to the midlatitudes, Poles, and tropical areas of elevation. Low-level clouds exist globally, but are underestimated in regions of persistent convection, persistent subsidence, and elevated terrain.

The overall lack of tropical cloudiness in the NR stems primarily from a difference in high-level clouds as shown in Fig. 6. As seen in Fig. 6c, the differences occur at all longitudes in the tropics, but especially over land areas. The area-averaged high cloud fraction is 19% smaller in the NR than in the CS/CAL data between 20°S and 20°N, but this number is inflated by the lack of cloudiness in the persistently convective regions over South America, central Africa, and Southeast Asia. The differences in these regions typically exceed 40% and peak at 65% over central Africa.

A lack of clouds is also seen in areas of subsidence associated with subtropical highs in the eastern Pacific and Atlantic, although the differences are considerably smaller in these regions than in the tropics. Further investigation showed that the seasonally averaged intensity of the subtropical highs in the NR fall within the climatological spread of the Modern Era Retrospective-Analysis for Research and Applications (MERRA; Rienecker et al. 2011), as shown in Fig. 9. The NR intensity falls within the MERRA spread in all three Southern Hemisphere oceanic subtropical highs, although it is closest to the minimum MERRA values, especially over the southern Pacific and Indian Oceans. This contrasts with the results in Fig. 6, where the lack of high clouds could improperly be inferred as being due to overly strong subsidence. In the NH, the intensity of the subtropical highs over the northern Pacific and northwestern Atlantic exceeds the MERRA spread. These areas correspond to two major climatological storm tracks (Hoskins and Hodges 2002). This misrepresentation of mean sea level pressure can be

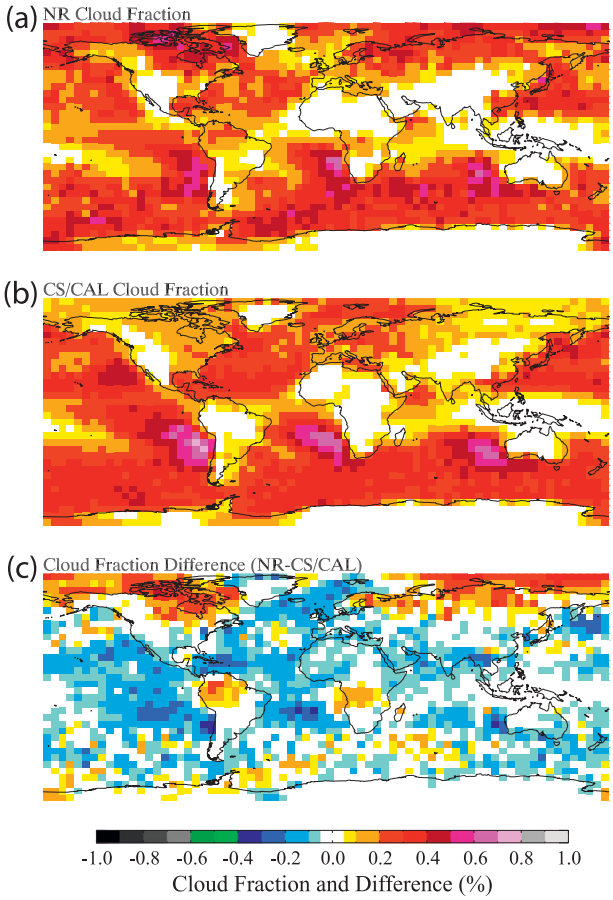

FIG. 8. As in Fig. 5, but for low-level clouds, defined as those having a cloud-top pressure greater than 700 hPa.

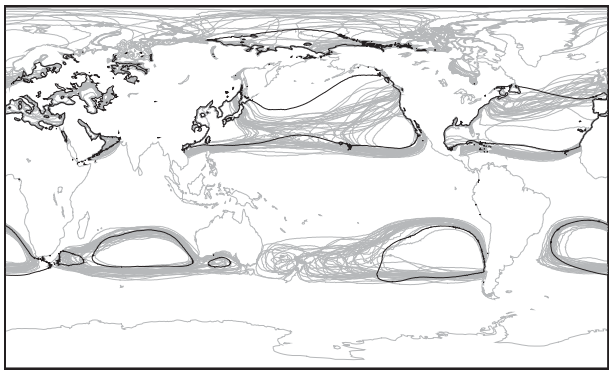

FIG. 9. Seasonally averaged 1016-hPa surface pressure contour for DJF of the NR (black) and each year of the MERRA reanalysis during 1979–2008 (gray).

the result of either fewer or weaker storms over the NR DJF season compared to MERRA. Over the polar regions, cloud amounts are generally overestimated in the NR, but local maxima do not explicitly align with those seen in Fig. 5. It is noted that the high-level layer is vertically thinner over the polar regions than over the midlatitudes and tropics as a result of a climatologically lower tropopause pressure–height (Hoinka 1998; Zangl and Hoinka 2001).

Of the three vertical layers, clouds in the midlevel best agree in the extrapolar regions (Fig. 7). Since the top-downward methodology only considers the highest cloud in both the CS/CAL and NR datasets, near-zero cloud fractions in the tropics and midlatitudes do not indicate that there are no clouds in this layer. The difference between the NR and CS/CAL data (Fig. 7c) at the midlevel illustrates the general deficiency in NR clouds seen in the tropics and midlatitudes in Fig. 5, although the difference is much smaller than at the upper-level. The small midlevel cloud amounts in each dataset (Figs. 7a,b) follow the distributions presented for HIRS and the Geoscience Laser Altimeter System (GLAS) reported by Wylie et al. (2007). Cloud fractions for this layer are larger over the polar regions than the extrapolar regions. When considering the difference between the two datasets, the maximum overestimation of cloud in the NR compared to CS/CAL occurs over the Antarctic. This corresponds to the Antarctic maximum seen in Fig. 5 and occurs over the points of highest elevation. The minima in total clouds in the NR seen in Fig. 5 over the southern polar region also correspond with differences in midlevel clouds in Fig. 7, such as near the Weddell Sea and the Ross Sea, but these are not as pronounced.

The overall underestimation of cloud fraction in the NR is further highlighted in the analysis of low cloud fraction in Fig. 8. Again, cloud fraction in the NR is most deficient over the tropical oceans, particularly the Atlantic and the eastern Pacific. In the convective regions of South America and central Africa, the NR actually shows more low clouds than the CS/CAL data. Since high clouds in these regions are dramatically underestimated in the NR (Fig. 6), more low clouds are sampled in the NR because of the top-downward methodology. The minimum differences aloft are larger than the maximum differences below, so these convective regions are still deficient overall (Fig. 5), as the sum of the cloud fractions in each vertical layer is equal to the overall fraction. The NR underestimates low clouds in the Northern Hemisphere midlatitudes primarily over the ocean compared to CS/CAL. Clouds in the Southern Hemisphere are also underestimated, but to a lesser degree than in the Northern Hemisphere. In the Antarctic, the lowest layer is volumetrically thin due to elevation and the minimal difference is seen between the NR and CS/CAL. The NR overestimates low cloud fraction in the Arctic, where the largest differences correspond spatially to the overall differences (Fig. 5).

5. Conclusions

This study examines the depiction of clouds, in terms of cloud fraction, in the December–February season of the ECMWF T511 nature run provided for the ''Joint OSSE'' effort. The DJF time frame is chosen for its relevance to other aspects of the development of an OSSE framework based on the Goddard Earth Observing System, version 5 (GEOS-5) atmospheric data assimilation system at the GMAO. The proper handling of clouds as part of the generation of realistic observations is essential to a successful OSSE.

The NR is shown to lack clouds globally. The largest underestimation of clouds is at the equator and lessens poleward until the difference changes sign, as cloud fraction is overestimated in the polar regions. These differences are larger in the Northern Hemisphere than in the Southern Hemisphere. While no comparison between the winter and summer seasons of the NR was possible in the context of the present study, the larger differences in cloud fraction seen in the Northern Hemisphere may relate to deficiencies in extratropical cyclone frequency or intensity in the NR. This speculation is based on the fact that the seasonally averaged contour of 1016-hPa surface pressure exceeded that of the MERRA reanalysis (Fig. 9). Either of these effects would result in an increased mean surface pressure and a lack of clouds in the NR. Further investigation of this anomaly would help verify the NR.

This study shows deficiencies in various elements of the cloud fraction fields from a so-called top-downward perspective. This perspective was chosen because most spaceborne observations, which dominate the global observing system in terms of data counts, observe clouds this way. Traditionally in data assimilation, observations affected by clouds are considered contaminated and are discarded. To match yield statistics in terms of used observations in data assimilation, a variety of methods could be used. Since clouds tend to exist in meteorologically significant areas (McNally 2002; Errico et al. 2007), simulated observations should contain cloud effects representative of the meteorological situations in the NR fields in which they are present.

The understatement of cloud presented in the context of this study does not render the NR unusable for an OSSE. For example, current GMAO efforts have employed a probabilistic model of clouds as a function of the NR cloud fraction to simulate infrared observations with realistic cloud effects. This method uses a tunable function that allows for the cloud effects on the observations to be adjusted to match realistic distributions seen in a real observing system. The cloud-affected observations generated this way are assumed to measure clouds that are blackbodies and infinitesimally thin. For atmospheric motion vections (AMVs), Masutani et al. (2010) uses locations based on a set of real observations, irrespective of nature run fields. The generation of AMVs as a function of both the NR cloud and water vapor fields requires the development of an advanced algorithm to produce measurement yields similar to those produced by feature-tracking algorithms used to generate actual AMVs (i.e., Menzel et al. 1983; Velden et al. 1997). The development of such an algorithm is under way at the GMAO (N. Prive 2011, personal communication).

While simulated observations can be compared to real observations to properly account for the deficiencies in the nature run fields, there is no preexisting baseline for future observation types without spaceborne heritage. An example of this is the Doppler wind lidar (DWL), which has been the subject of a number of OSSEs (i.e., Rohaly and Krishnamurti 1993; Stoffelen et al. 2006; Masutani et al. 2010). While measurement yields can be inferred from climatologies generated from existing spaceborne lidars, including CALIOP on *CALIPSO* and GLAS on the *Ice, Cloud, and land Elevation Satellite* (*ICESat*), such instruments typically produce measurements at much finer resolutions than (existing) NRs. Masutani et al. (1999) adjusted low-level clouds based on ground observations and rising motion in the nature run. Adjustments were conducted based on known model problems. Also, DWL instrument models (i.e., Marseille and Stoffelen 2003) are advanced enough to consider backscatter and extinction, which are functions of the ice and liquid water contents. However, in the event that a cloud fraction is zero, the water content variables must be adjusted from zero to nonzero, which is a nontrivial problem.

The results presented here are for the benefit of the ''Joint OSSE'' project. The issues discussed have relevance to the simulation of nearly every spaceborne observation type, and they must be addressed in the development of an OSSE framework. The lessons learned in this study will be applied to future OSSE verification as the simulation of observations from this NR is under way in multiple efforts. This effort could be expanded both to different seasons. It could also be expanded to include an instrument model to better understand the effects of the cloud liquid and ice water fields that correspond to the cloud fraction fields. Similarly, the methods used in this study will be applicable to future NRs, especially as increases in computational resources allows for the generation of much higher-resolution datasets.

Acknowledgments. The research presented benefitted greatly from discussions with Gert-Jan Marseille and Ad Stoffelen of KNMI. This work was supported under NASA WBS 281945.02.19.01.12.

REFERENCES

Andersson, E., and M. Masutani, 2010: Collaboration on Observing System Simulation Experiments (Joint OSSE). *ECWMF Newsletter,* No. 123, ECMWF, Reading, United Kingdom, 14–16. [Available online at http://www.emc.ncep.noaa.gov/research/JointOSSEs/publications/JOSSE-Publication-files/Andersson_JOSSE_ECMWF_News_No123.pdf.]

Chepfer, H., S. Bony, D. Winker, M. Chiriaco, J. L. Dufresne, and G. Sèze, 2008: Use of CALIPSO lidar observations to evaluate the cloudiness simulated by a climate model. *Geophys. Res. Lett.,* **35,** L15704, doi:10.1029/2008GL034207.

Derber, J. C., and W.-S. Wu, 1998: The use of TOVS cloud-cleared radiances in the NCEP SSI analysis system. *Mon. Wea. Rev.,* **126,** 2287–2299.

Errico, R. M., G. Ohring, P. Bauer, B. Ferrier, J.-F. Mahfouf, J. Turk, and F. Weng, 2007: Assimilation of satellite cloud and precipitation observations in numerical weather prediction models: Introduction to the JAS Special Collection. *J. Atmos. Sci.,* **64,** 3737–3741.

Geleyn, J.-F., and A. Hollingsworth, 1979: An economical analytical method for the computation of the interaction between scattering and line absorption of radiation. *J. Atmos. Phys.,* **52,** 1–16.

Hoinka, K. P., 1998: Statistics of the global tropopause pressure. *Mon. Wea. Rev.,* **126,** 3303–3325.

Hoskins, B. J., and K. I. Hodges, 2002: New perspectives on the Northern Hemisphere winter storm tracks. *J. Atmos. Sci.,* **59,** 1041–1061.

Mace, J., and Q. Zhang, 2008: 2B-GEOPROF-LIDAR interface control document. 2B-GEOPROF-LIDAR product version: 003, algorithm version 1.1, 13 pp.[Available online at http://www.cloudsat.cira.colostate.edu/icd_pdf.php?avid=115&pvids=214.]

Marseille, G. J., and A. Stoffelen, 2003: Simulation of wind profiles from a space-borne Doppler wind lidar. *Quart. J. Roy. Meteor. Soc.,* **129,** 3079–3098.

Masutani, M., K. A. Campana, S. J. Lord, and S.-K. Yang, 1999: Note on cloud cover of the ECMWF nature run used for OSSE/NPOESS Project. NCEP Office Note 427, 48 pp.

——, and Coauthors, 2009: International Collaborative Joint OSSEs—Toward reliable and timely assessment of future observing systems. Preprints, *Anthony J. Hollingsworth Symp.,* Phoenix, AZ, Amer. Meteor. Soc., P1.2. [Available online at http://ams.confex.com/ams/pdfpapers/149641.pdf.]

——, and Coauthors, 2010: Observing system simulation experiments at the National Centers for Environmental Prediction. *J. Geophys. Res.,* **115,** D07101, doi:10.1029/2009JD012528.

McNally, A. P., 2002: A note on the occurrence of cloud in meteorologically sensitive areas and the implications for advanced infrared sounders. *Quart. J. Roy. Meteor. Soc.,* **128,** 2551–2556.

——, and P. D. Watts, 2003: A cloud detection algorithm for high-spectral-resolution infrared sounders. *Quart. J. Roy. Meteor. Soc.,* **129,** 3411–3423.

Menzel, W. P., W. L. Smith, and T. R. Stewart, 1983: Improved cloud motion wind vector and altitude assignment using VAS. *J. Climate Appl. Meteor.,* **22,** 377–384.

Partain, P., 2010: CloudSat ECMWF-AUX auxiliary data process description and interface control document. Algorithm version 3.0, 8 pp. [Available online at http://cloudsat.cira.colostate.edu/ICD/ECMWF-AUX/ECMWF-AUX_PDICD_3.0.pdf.]

Price, J. C., 1991: Timing of NOAA afternoon passes. *Int. J. Remote Sens.,* **12,** 193–198.

Reale, O., J. Terry, M. Masutani, E. Andersson, L. P. Riishojgaard, and J. C. Jusem, 2007: Preliminary evaluation of the European Centre for Medium-Range Weather Forecasts' (ECMWF) nature run over the tropical Atlantic and African monsoon region. *Geophys. Res. Lett.,* **34,** L22810, doi:10.1029/2007GL031640.

Rienecker, M. M., and Coauthors, 2011: MERRA: NASA's Modern-Era Retrospective Analysis for Research and Applications. *J. Climate,* **24,** 3624–3648.

Rohaly, G. D., and T. N. Krishnamurti, 1993: An Observing System Simulation Experiment for the Laser Atmospheric Wind Sounder (LAWS). *J. Appl. Meteor.,* **32,** 1453–1471.

Rossow, W. B., and R. A. Schiffer, 1991: ISCCP cloud data products. *Bull. Amer. Meteor. Soc.,* **72,** 2–20.

Smith, W. L., and C. M. R. Platt, 1978: Comparison of satellite-deduced cloud heights with indications from radiosonde and ground-based laser measurements. *J. Appl. Meteor.,* **17,** 1796–1802.

Stephens, G. L., and Coauthors, 2008: CloudSat mission: Performance and early science after the first year of operation. *J. Geophys. Res.,* **113,** D00A18, doi:10.1029/2008JD009982.

Stoffelen, A., G. J. Marseille, F. Bouttier, D. Vasiljevic, S. de Haan, and C. Cardinali, 2006: ADM-Aeolus Doppler wind lidar Observing System Simulation Experiment. *Quart. J. Roy. Meteor. Soc.,* **132,** 1927–1947.

Velden, C. S., C. M. Hayden, S. J. Nieman, W. P. Menzel, S. Wanzong, and J. S. Goerss, 1997: Upper-tropospheric winds derived from geostationary satellite water vapor observations. *Bull. Amer. Meteor. Soc.,* **78,** 173–195.

Weisz, E., J. Li, W. P. Menzel, A. K. Heidinger, B. H. Kahn, and C.-Y. Liu, 2007: Comparison of AIRS, MODIS, CloudSat, and CALIPSO cloud top height retrievals. *J. Geophys. Res.,* **34,** L17811, doi:10.1029/2007GL030676.

Wilkinson, J. M., R. J. Hogan, A. J. Illingworth, and A. Benedetti, 2008: Use of a lidar forward model for global comparisons of cloud fraction between the ICESat lidar and the ECMWF model. *Mon. Wea. Rev.,* **136,** 3742–3759.

Winker, D. M., W. H. Hunt, and M. J. McGill, 2007: Initial performance assessment of CALIOP. *Geophys. Res. Lett.,* **34,** L19803, doi:10.1029/2007GL030135.

Wylie, D. P., and W. P. Menzel, 1999: Eight years of high cloud statistics using HIRS. *J. Climate,* **12,** 170–184.

——, ——, H. M. Woolf, and K. I. Strabala, 1994: Four years of global cirrus cloud statistics using HIRS. *J. Climate,* **7,** 1972–1986.

——, E. Eloranta, J. D. Spinhirne, and S. P. Palm, 2007: A comparison of cloud cover statistics from the GLAS lidar with HIRS. *J. Climate,* **20,** 4968–4981.

Zangl, G., and K. P. Hoinka, 2001: The tropopause in the polar regions. *J. Climate,* **14,** 3117–3139.